



## Density variability at scales typical of gravity waves observed in Mars' thermosphere by the MGS accelerometer

John E. Creasey,<sup>1</sup> Jeffrey M. Forbes,<sup>1</sup> and Gerald M. Keating<sup>2</sup>

Received 15 July 2006; revised 25 September 2006; accepted 4 October 2006; published 30 November 2006.

[1] Examination of the small-scale density perturbations in Mars' thermosphere inferred from Mars Global Surveyor (MGS) accelerometer data reveals wave-like structures consistent with gravity waves. The structures are interpreted to be horizontal with dominant wavelengths of 100–300 km observed along the orbital path. Density perturbations are significantly stronger in winter versus spring/summer, suggesting that the zonal mean winds play a major role in filtering these waves. There is also evidence of possible modulation by the mean winds due to local time differences. No correlation is found with the underlying topography, a source region on Earth for gravity waves. In fact, density perturbations in the northern hemisphere are observed to be greater than those in the southern hemisphere, which has a higher orographic variance. Over the Martian tropics, an observed source region for gravity waves, density perturbations are again not elevated, leaving questions on how gravity waves observed in the lower atmosphere are related to those observed in the thermosphere. **Citation:** Creasey, J. E., J. M. Forbes, and G. M. Keating (2006), Density variability at scales typical of gravity waves observed in Mars' thermosphere by the MGS accelerometer, *Geophys. Res. Lett.*, 33, L22814, doi:10.1029/2006GL027583.

### 1. Introduction

[2] Gravity waves are an ubiquitous feature of planetary atmospheres. In Earth's atmosphere, gravity waves play an extremely important role in defining the circulation and thermal structure of the mesosphere [e.g., *McLandress*, 1998]. Gravity waves break in Earth's mesosphere, deposit momentum into the mean flow, and as a result reverse the direction of the zonal mean wind jets around 65–75 km. The zonal forcing combined with the Coriolis force drives a meridional circulation with strong upwelling (downwelling) and adiabatic cooling (subsidence heating) in the summer (winter) hemisphere, driving the mesopause region far from radiative equilibrium. Wave breaking also contributes significantly to turbulent mixing in the region.

[3] The influence of gravity waves on the middle and upper atmosphere dynamics of Mars is not nearly as well established as for Earth, although numerical models have attempted to parameterize the effects of orographically-generated gravity waves [*Théodore et al.*, 1993; *Joshi et*

*al.*, 1995; *Collins et al.*, 1997; *Forget et al.*, 1999]. However, a recent analysis of Mars Global Surveyor (MGS) radio occultation temperature profiles [*Creasey et al.*, 2006] shows that the global distribution of gravity wave energy near 25 km in Mars' atmosphere does not correlate well with source distributions that would be expected on the basis of topographic generation of waves. This leaves open the question of the primary source mechanisms and source spectra (i.e., distribution of phase speeds).

[4] Gravity waves have been observed [e.g., *Hinson and Jenkins*, 1995] and cited as potentially important for the dynamics of Venus' lower and middle atmosphere [*Schubert and Waterscheid*, 1984; *Hou and Farrell*, 1987; *Leroy and Ingersoll*, 1994], and have even been found to be a common characteristic of Venus' thermosphere [*Kasprzak et al.*, 1988]. The effects of upward-propagating gravity waves on Earth's thermosphere are not even well-established and are difficult to separate from waves emanating from auroral sources [*Forbes et al.*, 1995]. In the thermospheres of Venus and Mars, however, most wave activity observed is likely to originate in their lower atmospheres, and therefore represents a means of vertically coupling energy and momentum.

[5] The characteristics of gravity waves in Mars' thermosphere are currently unknown, and it is our objective in this paper to provide some insight into this problem through examination of in-situ density measurements between 100 and 170 km by the accelerometer on MGS. This work complements a previous study by the authors [*Creasey et al.*, 2006] who utilized MGS radio occultation measurements to delineate the gravity wave energy emanating upward from the lower atmosphere. These combined data sets can begin to provide some constraints on parameterization of gravity wave effects in models of large-scale atmosphere dynamics, while in addition providing information on atmospheric variability relevant to future exploration activities involving aerobraking, aerocapture, and entry, descent and landing (EDL).

### 2. Data Analysis

[6] The MGS accelerometer experiment provided measurements of Mars' thermospheric densities during Phase I (September 1997–March 1998) and Phase II (September 1998–February 1999) of MGS aerobraking operations. The combined Phase I and Phase II measurements, obtained from the NASA Planetary Data System [*Keating et al.*, 2001], have provided over 800 inbound-outbound density profiles ranging from about 100 to 170 km altitude and covering all latitudes from 60°N to the South Pole. Figure 1 shows the relatively even geographical distribution of measurements. Phase I measurements were taken in northern late autumn and early winter (latitude 30°N–60°N,

<sup>1</sup>Department of Aerospace Engineering Sciences, University of Colorado, Boulder, Colorado, USA.

<sup>2</sup>Joint Institute for Advancement of Flight Sciences, George Washington University, NASA Langley Research Center, Hampton, Virginia, USA.

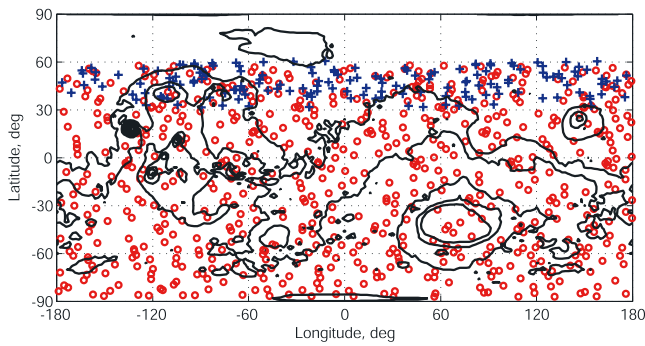


**Figure 1.** Distribution of accelerometer measurements relative to Martian topography. Each marker represents the periapsis location for one orbit, with blue plus symbols indicating Phase I and red circles indicating Phase II. Contour intervals are spaced every 3000 m.

areocentric longitude ( $L_s$ , 180–300°) of Martian Year (MY) 23 [Clancy *et al.*, 2000], while Phase II measurements spanned northern early spring to southern winter (latitude 60°N–87°S,  $L_s$  30–90°) of MY 24. Local true solar times (LTST) ranged from approximately 1100 to 1800 in Phase I and from 1500 to 0200 in Phase II. Figure 2a shows the progression of  $L_s$ , periapsis latitude, and LTST during Phases I and II.

[7] MGS accelerometer data have previously been used to study tidal waves [e.g. Withers *et al.*, 2003; Forbes *et al.*, 2004], but until only recently [Withers, 2006], had not been used to investigate smaller-scale wave-like perturbations. To

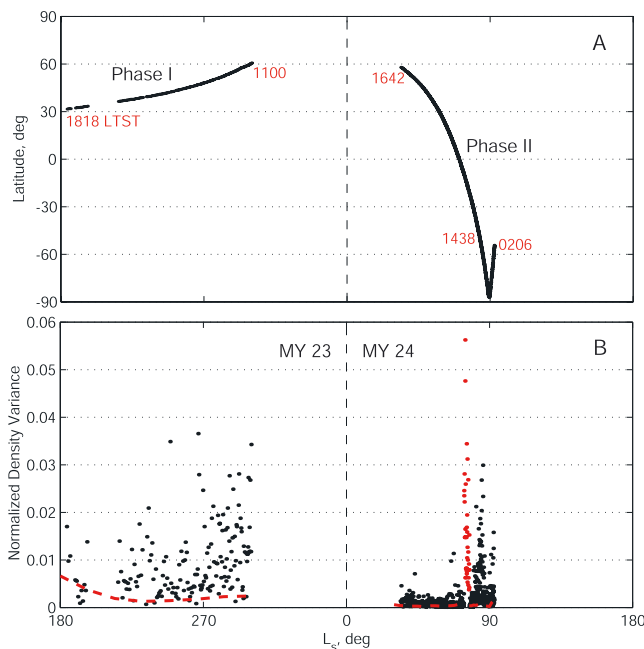


**Figure 2.** (a) Latitude distribution of MGS accelerometer measurements for Phase I (Martian Year (MY) 23) and Phase II (MY 24) with selected LTST annotated. (b) Variance (wave power) of the density fluctuations computed for each profile. The red markers indicate unused data on orbits 911–961, and the dashed red lines represent the variance due to measurement uncertainty.

understand the structure of these waves, the data analysis herein follows the approach used by Fritts *et al.* [1989, 1993] with Space Shuttle accelerometer data collected during reentry and that used by Kasprzak *et al.* [1988] with PVO spectrometer data collected during orbiter entry at Venus.

[8] All orbits with valid density profiles were used in the analysis, with the notable exclusion of profiles collected on orbits 911–961. Although these profiles possess strong wave-like perturbations (red data points in Figure 2b), they had been identified on the PDS site as anomalous and therefore are not discussed in the results section. Each profile contains inferred densities reported each second using 7-second and 40-second sampling. A typical example is shown in Figure 3a. The density perturbation  $\rho'$  is calculated by subtracting the mean density  $\bar{\rho}$ , taken here to be the 40-second averaged density data, from the 7-second averaged data. The fractional density fluctuation,  $\rho'/\bar{\rho}$ , normalizes the perturbations to the mean density (Figure 3b). Mean and quadratic trends were removed from the fractional density fluctuation. The quadratic trend is an artifact of the density gradient difference in the 7-second and 40-second data caused by the non-circular aerobraking orbit. For each profile, data were reduced to  $\pm 100$  seconds about periapsis, which for a typical mid-latitude profile corresponds to roughly 12–15 degrees in latitude, 2 degrees in longitude, and 700–900 km along the orbital track. The height span for the reduced profile ranged from 15 km at the start of aerobraking to less than 1 km at the end.

[9] Measurement uncertainties, which include errors due to data noise and natural variability, were evaluated using the  $1\sigma$  errors in the 40-second density data [Keating *et al.*, 2001]. Height-averaged measurement errors of 0.2 to

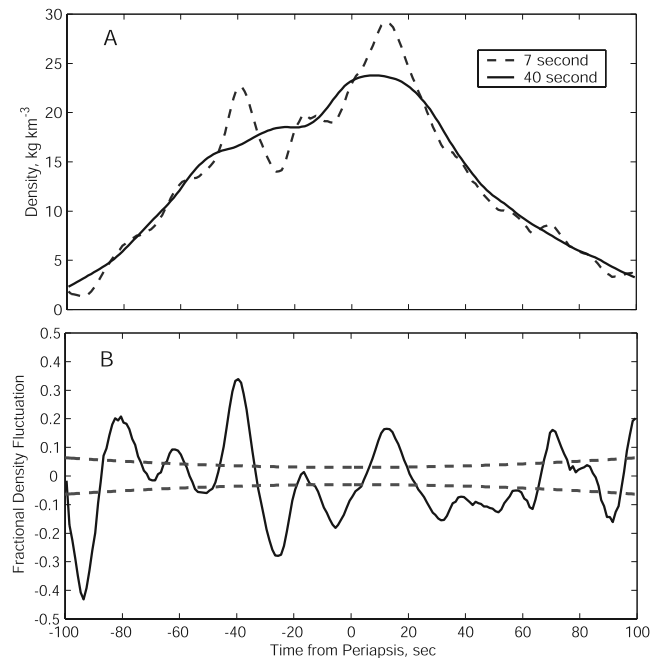


**Figure 3.** Example accelerometer profile P0179 showing (a) 7-second and 40-second averaged density data, and (b) corresponding fractional density fluctuation. The dashed lines in Figure 3b represent the height-averaged  $1\sigma$  measurement errors.

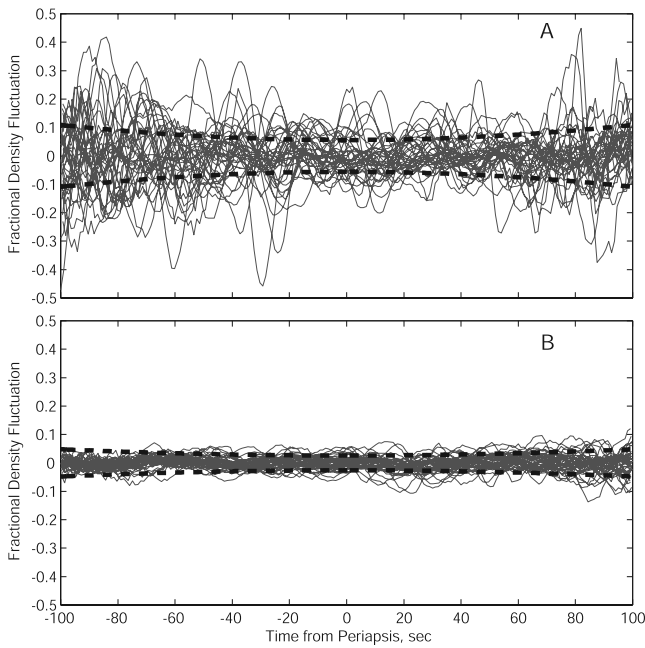


**Figure 4.** Seasonal contrast between (a) orbits 5–66, periapsis at  $32^{\circ}\text{N}$ – $40^{\circ}\text{N}$  latitude, 1500–1800 LTST, and areocentric longitude ( $L_s$ )  $183$ – $237^{\circ}$  (northern autumn), and (b) orbits 674–718, periapsis at  $32^{\circ}\text{N}$ – $40^{\circ}\text{N}$  latitude, 1530–1600 LTST, and  $L_s$   $51$ – $57^{\circ}$  (northern spring). Dashed lines depict  $1\sigma$  measurement errors.

$0.6 \text{ kg/km}^3$  are consistent with Tolson *et al.* [2000] and correspond to 2% and 10% of mean density at heights of 110 km and 140 km respectively.

[10] Wave spectral power was analyzed using Parseval's relation for the Discrete Fourier Transform (DFT) [Oppenheim and Schaffer, 1989], which states that the spectral power for a profile is related to the variance of the zero-mean fractional density fluctuation. Figure 2b shows the variance calculated for each profile in Phases I and II. Note that in computing variance, measurement error was not separated from wave spectral power. Spectra of the fractional density fluctuations were also computed and averaged to isolate the spectral components of the perturbations.

### 3. Results

[11] Inspection of the fluctuation variances in Figure 2 shows that elevated density perturbations occurred throughout Phase I and in the latter part of Phase II with a relatively quiet period for the first half of Phase II. Given the progression of the measurements through  $L_s$ , latitude, and LTST, we are able to contrast periods of density perturbations by season, hemisphere, and local time.

[12] Figure 4 compares fractional density fluctuations at northern mid-latitudes, at the same local time, but in different seasons. In northern autumn (Figure 4a), density fluctuations sometimes exceed 30%; yet in northern spring (Figure 4b) density fluctuations rarely approach 5%. Mean perturbation variance is 13 times higher in northern autumn. These results may be explained by filtering by the zonal mean winds associated with the middle-atmosphere jets. From the Mars Climate Database [Forget *et al.*, 1999],

westward-propagating waves may be encountering a critical level in spring and summer, but as the jet decreases towards autumn equinox, these waves may propagate to the thermosphere.

[13] Significant density fluctuations are observed in both northern winter at northern latitudes and southern winter at southern latitudes as depicted in Figures 5a and 5b. Latitude bands are comparable ( $54^{\circ}\text{N}$ – $60^{\circ}\text{N}$  versus  $54^{\circ}\text{S}$ – $65^{\circ}\text{S}$ ), but local times differ slightly (1100 versus 1500 LTST). Although density fluctuations are elevated in both hemispheres, mean variance is 50% higher in the northern hemisphere. Given the higher orographic variance in the southern hemisphere, this result suggests that small-scale waves observed in the thermosphere may not be heavily influenced by the underlying topography. Figures 5b and 5c compare density fluctuations in southern winter near  $60^{\circ}\text{S}$  latitude at different local times. At 1500 LTST, variance is

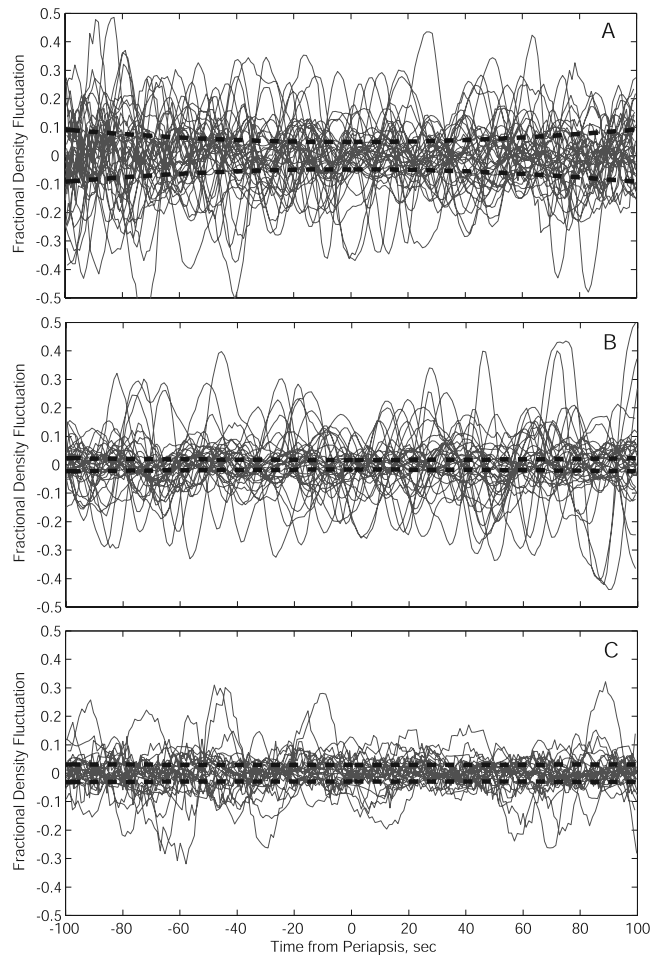


**Figure 5.** Northern hemisphere winter/southern hemisphere winter contrast between (a) orbits 158–201, periapsis at  $54^{\circ}\text{N}$ – $60^{\circ}\text{N}$  latitude, 1100–1200 LTST, and  $L_s$   $286$ – $300^{\circ}$  (24–47 sols past northern winter solstice), and (b) orbits 1081–1115, periapsis at  $54^{\circ}\text{S}$ – $65^{\circ}\text{S}$  latitude, 1500 LTST, and  $L_s$   $84$ – $86^{\circ}$  (8–12 sols before southern winter solstice). Local time contrast between Figure 5b and (c) orbits 1254–1283, periapsis at  $54^{\circ}\text{S}$ – $65^{\circ}\text{S}$ , 0200 LTST, and  $L_s$   $91$ – $93^{\circ}$  (southern winter). Dashed lines depict  $1\sigma$  measurement errors.

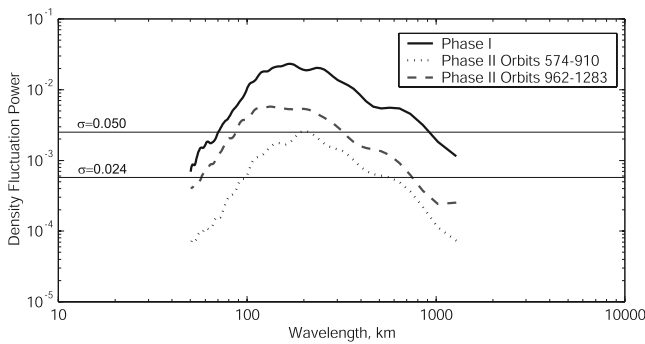


**Figure 6.** Averaged spectra of density fluctuations observed along the orbital path. Spectra are shown for Phase I, Phase II northern spring and tropics (orbits 574–910), and Phase II southern winter (orbits 962–1283). Horizontal lines represent white noise with standard deviations equivalent to mean fractional density fluctuation errors of 5.0% and 2.4% for Phase I and II respectively.

two times greater than at 0200 LTST, which may be evidence of a difference between daytime and nighttime filtering by tidal related winds.

[14] Because the above comparisons focus on distinct time periods, it is possible that the results may have been influenced by temporal events. One such event, the Noachis dust storm, occurred during Phase I. During the dust storm onset and decay, densities increase three-fold due to atmospheric expansion [Bougher *et al.*, 1999], but no noticeable change is observed in wave-like density perturbations. Further, no correlation is found with the regional and local dust storms reported by Smith *et al.* [2000], although it should be noted that the Thermal Emission Spectrometer (TES) used to collect dust opacity data was not operated during Phase II of aerobraking.

[15] Finally, no correlation is found between the location of elevated density perturbations and the expected source regions for gravity waves. From Creasey *et al.* [2006], gravity waves are observed to be much stronger in the lower atmosphere over the Martian tropics and, to a lesser degree, over areas of significant topography. In the thermosphere, there appears to be no difference between tropical and extratropical density perturbations, although the availability of accelerometer data over the tropics is limited. More data are needed to better understand how gravity waves observed in the lower atmosphere are associated with the gravity waves observed in the thermosphere.

[16] Spectra of fractional density fluctuations reveal dominant wavelengths of 100–300 km along the orbital path. Following the arguments of Fritts *et al.* [1989], the observed spectra are presumed due to horizontal rather than vertical variations. Because the direction of wave propagation relative to the orbital path is not known, the effective horizontal wavelength may be less than that observed. The horizontal scales on the order of 100–300 km are consistent with observations of gravity waves [Fritts, 1984] and are much too small to be representative of tides or planetary waves. Figure 6 shows averaged spectra for three periods - Phase I, Phase II northern spring, and Phase II southern winter. Relative power varies due to differences in density perturbations discussed above, but the averaged spectra are

similar across the three periods, indicating that the waves observed in the thermosphere are of the same species irrespective of filtering.

#### 4. Conclusions

[17] Analysis of the density perturbations observed by the MGS accelerometer has begun to reveal the structure of gravity waves in the thermosphere and has provided insight into how gravity waves which propagate to the thermosphere are filtered and modulated by season and perhaps by local time of day. These results have practical value to aerobraking activities. To avoid density variability in the thermosphere, aerobraking should occur in spring/summer periods when gravity waves may be preferentially filtered by the mean winds. The results herein can also be used to constrain parameterization of gravity waves in Mars atmospheric dynamic models, whose fidelities can be improved with more observational data, such as accelerometer data from Mars Odyssey and MRO at comparable resolution. Further observations and modeling studies will ultimately lead to a better understanding of the role of gravity waves in the dynamics of the middle and upper atmosphere of Mars.

[18] **Acknowledgments.** This work was supported by grant NNG04GJ97G from the NASA Mars Data Analysis Program to the University of Colorado.

#### References

- Bougher, S., G. Keating, R. Zurek, J. Murphy, R. Haberle, J. Hollingsworth, and R. T. Clancy (1999), Mars Global Surveyor aerobraking: Atmospheric trends and model interpretation, *Adv. Space Res.*, 23, 1887–1897.
- Clancy, R. T., B. J. Sandor, M. J. Wolff, P. R. Christensen, M. D. Smith, J. C. Pearl, B. J. Conrath, and R. J. Wilson (2000), An interpretation of ground-based millimeter, MGS TES, and Viking atmospheric temperature measurements and dust loading in the global Mars atmosphere, *J. Geophys. Res.*, 105, 9553–9571.
- Collins, M., S. R. Lewis, and P. L. Read (1997), Gravity wave drag in a global circulation model of the Martian atmosphere: Parametrisation and validation, *Adv. Space Res.*, 44, 1395–1409.
- Creasey, J. E., J. M. Forbes, and D. P. Hinson (2006), Global and seasonal distribution of gravity wave activity in Mars' lower atmosphere derived from MGS radio occultation data, *Geophys. Res. Lett.*, 33, L01803, doi:10.1029/2005GL024037.
- Forbes, J. M., F. A. Marcos, and F. Kamalabadi (1995), Wave structures in lower thermosphere density from Satellite Electrostatic Triaxial Accelerometer (SETA) measurements, *J. Geophys. Res.*, 100, 14,693–14,702.
- Forbes, J. M., X. Zhang, M. Angelats i Coll, and G. M. Keating (2004), Nonmigrating tides in the thermosphere of Mars: A quasi-empirical description, *Adv. Space Res.*, 34, 1690–1695.
- Forget, F., F. Hourdin, R. Fournier, C. Hourdin, O. Talagrand, M. Collins, S. R. Lewis, P. L. Read, and J.-P. Huot (1999), Improved general circulation models of the Martian atmosphere from the surface to above 80 km, *J. Geophys. Res.*, 104, 24,155–24,176.
- Fritts, D. C. (1984), Gravity wave saturation in the middle atmosphere: A review of theory and observations, *Rev. Geophys.*, 22, 275–308.
- Fritts, D. C., R. C. Blanchard, and L. Coy (1989), Gravity wave structure between 60 and 90 km inferred from space shuttle reentry data, *J. Atmos. Sci.*, 46, 423–434.
- Fritts, D. C., D. Wang, and R. C. Blanchard (1993), Gravity wave and tidal structures between 60 and 140 km inferred from space shuttle reentry data, *J. Atmos. Sci.*, 50, 837–849.
- Hinson, D. P., and J. M. Jenkins (1995), Magellan radio occultation measurements of atmospheric waves on Venus, *Icarus*, 114, 310–327.
- Hou, A. Y., and B. F. Farrell (1987), Superrotation induced by critical-level absorption of gravity waves on Venus: An assessment, *J. Atmos. Sci.*, 44, 1049–1061.
- Joshi, M. M., B. N. Lawrence, and S. R. Lewis (1995), Gravity wave drag in three-dimensional atmospheric models of Mars, *J. Geophys. Res.*, 100, 21,235–21,245.

- Kasprzak, W. T., A. E. Hedin, H. G. Mayr, and H. B. Niemann (1988), Wavelike perturbations observed in the neutral thermosphere of Venus, *J. Geophys. Res.*, *93*, 11,237–11,245.
- Keating, G. M., R. H. Tolson, J. L. Hanna, R. F. Beebe, J. R. Murphy, and L. F. Huber (2001), MGS-M-ACCEL-5-PROFILE-V1.1, [http://atmos.nmsu.edu/PDS/data/mgsa\\_0002/](http://atmos.nmsu.edu/PDS/data/mgsa_0002/), NASA Planet. Data Syst., Greenbelt, Md.
- Leroy, S. S., and A. P. Ingersoll (1994), Convective generation of gravity waves in Venus' atmosphere: Gravity wave spectrum and momentum transport, *J. Atmos. Sci.*, *52*, 3717–3737.
- McLandress, C. (1998), On the importance of gravity waves in the middle atmosphere and their parameterization in general circulation models, *J. Atmos. Sol. Terr. Phys.*, *60*, 1357–1383.
- Oppenheim, A. V., and R. W. Schaffer (1989), *Discrete-Time Signal Processing*, Prentice-Hall, Upper Saddle River, N. J.
- Schubert, G., and R. L. Waterscheid (1984), Propagation of small-scale acoustic-gravity waves in the Venus atmosphere, *J. Atmos. Sci.*, *41*, 1202–1213.
- Smith, M. D., J. C. Pearl, B. J. Conrath, and P. R. Christensen (2000), Mars Global Surveyor Thermal Emission Spectrometer (TES) observations of dust opacity during aerobraking and science phasing, *J. Geophys. Res.*, *105*, 9539–9552.
- Théodore, B., E. Lellouch, E. Chassefière, and A. Hauchecorne (1993), Solstitial temperature inversions in the Martian middle atmosphere: Observational clues and 2-D modeling, *Icarus*, *105*, 512–528.
- Tolson, R. H., G. M. Keating, S. N. Noll, D. T. Baird, and T. J. Shellenberg (2000), Utilization of Mars Global Surveyor accelerometer data for atmospheric modeling, *Adv. Astronaut. Sci.*, *103*, 1329–1346.
- Withers, P. (2006), Mars Global Surveyor and Mars Odyssey accelerometer observations of the Martian upper atmosphere during aerobraking, *Geophys. Res. Lett.*, *33*, L02201, doi:10.1029/2005GL024447.
- Withers, P., S. W. Bougher, and G. M. Keating (2003), The effects of topographically-controlled thermal tides in the Martian upper atmosphere as seen by the MGS accelerometer, *Icarus*, *164*, 14–32.

---

J. E. Creasey and J. M. Forbes, Department of Aerospace Engineering Sciences, University of Colorado, Campus Box 429, Boulder, CO 80309-0429, USA. (john.creasey@colorado.edu; forbes@colorado.edu)

G. M. Keating, Joint Institute for Advancement of Flight Sciences, George Washington University, NASA Langley Research Center, Hampton, VA 23681, USA. (g.m.keating@larc.nasa.gov)